The dual information preserving method for stiff reacting flows

Li Liu[1], Yiqing Shen[1,2]

[1] *LHD, Institute of Mechanics, Chinese Academy of Sciences, Beijing 100190, China*

[2] *School of Engineering Science, University of Chinese Academy of Sciences, Beijing 100049, China*

Abstract

In this paper, we construct a new numerical method to solve the reactive Euler equations to cure the numerical stiffness problem. First, the species mass equations are decoupled from the reactive Euler equations, and they are further fractionated into the convection step and reaction step. In the species convection step, by introducing two kinds of virtual Lagrangian point (cell-point and particle-point), a dual information preserving (DIP) method is proposed to resolve the convection characteristics. In this new method, the information (including the transport value and the relative location to the centre of current cell) of cell-point and paticle-point are updated according to the velocity field. By using the DIP method, the incorrect activate position of the reaction, which may be caused by the numerical dissipation, can be effectively avoided. In addition, a numerical perturbation method is also developed to solve the fractionated reaction step (ODE equation) to improve the stability and efficiency. A series of numerical examples are presented to validate the accuracy and robustness of the new method.

Keywords: Stiff reacting flow, Dual information preserving method, Numerical pertutbation method, Shock-capturing scheme

1. Introduction

In simulating problems governed by reactive Euler equations, such as combustion and high speed chemical reaction, the difference of the timescales of reaction and convection which limits both the time step and grid spacing may cause the numerical stiffness problems, for example, the spurious numerical propagation phenomenon of the shock waves in flow fields[**?** **?** **?**]. In order to attenuate the influence of limited time step, the implicit time method or fraction step method is usually used to calculate the reaction ODE equations. However, if the mesh is not fine enough, the time method cannot remove the incorrect reaction activation caused by the spatial discretization, especially in the flow with shock waves. This is because the numerical dissipation introduced to capture shocks smears the shock front and also leads to the reaction activation in incorrect cells. Although the applications of high order shock capturing schemes can effectively

*Correspondence to: Yiqing Shen, LHD, Institute of Mechanics, Chinese Academy of Sciences, Beijing 100190, China. E-mail: yqshen@imech.ac.cn

reduce numerical dissipation and sharpen the discontinuity, the incorrect reaction activation and spurious propagation may still occur.

Wang et al.[**?**] gave a comprehensive overview of the last two decades of efforts contributed to overcome the spurious numerical phenomenon. Bao and Jin [**?** **?** **?**] developed a random projection method in the reaction terms to capture the detonations, but the assumption of a priori stiff source limits the application of this method. Zhang et al.[**?**] proposed an equilibrium state method (ESM) by using appropriate equilibrium states to activate the stiff source terms. The main defect of ESM in application is that it is difficult to determine the equilibrium states, especially in complex chemical system. Based on the idea of Harten ENO subcell resolution method[**?**], Chang[**?**] developed a finite volume ENO method in the convection step, while Wang et al.[**?** **?**] proposed high order finite difference methods with subcell resolution reconstructing the reaction step. However, as pointed out by Yee et al.[**?**], the subcell resolution method and its nonlinear filter counterparts[**?**] can delay the onset of the wrong speed of propagation for the stiff detonation problem with coarse grids and moderate stiff source terms, but this kind of method has additional spurious behavior as the grid is refined and the stiffness is further increased.

Ideally, the shock wave front can be regarded as an interface, hence, the interfacial tracking methods, such as the level set method, the VOF method and the front tracking method, seem as a good option for simulating reacting flows. In fact, they have been used in the premixed combustion with the instantaneous flame viewed as an infinitely thin interface between fresh and burned gases[**?** **?**], and also used in alleviating the nonphysical phenomena[**?**] in the simple two-phases detonations by tracking the inert shock as an interface. However, since the general chemical dynamic model comprises of multi-species with a finite rate of reactions, there is a continuous reacting region other than a traditional two-phases interface, hence, these interfacial tracking methods mentioned above cannot solve the stiff problem generated in chemical flows well.

For solving the interface/free surface fluid flow problems, the marker and cell (MAC) method is regarded as the basis of interfacial tracking techniques[**?**]. The essence of the MAC method is the Lagrangian virtual marker particles and the cells defined on an Eulerian grid. Marker particles, often as many as 16 per cell, are moved from their coordinates at time t_n to their new coordinates at time t_{n+1} according to the newly computed velocity u at the cell centre. The cell classification is updated at each time step using information provided by the virtual Lagrangian mesh constituted by the marker particles. The MAC method has been applied to interface/free surface flow problems successfully[**?** **?** **?**]. The main advantages of the MAC method are that it eliminates all logic problems associated with interfaces and readily extended to three-dimensional computations. However, the storage increase significantly, because a large number of particle coordinates must be stored. Another limitation in the MAC method as well as in the Level-set and the VOF methods is that it is difficult to extend to the case that the interface (free surface) is generated by the flow itself, such as the shock wave and the chemical reaction.

In this paper, by introducing two kinds of virtual Lagrangian points, we propose a dual information preserving method to cure the spurious numerical propagation phenomenon in simulating chemical reacting

flows. In this method, the information includes the transport value and the relative coordinates to the center of the Eulerian cell containing the virtual point. The species mass fraction equations are first decoupled from the reactive Euler equations, and then they are further fractionated into the convection step and reaction step. In the species convection step, one Lagrangian particle-point and one Lagrangian cell-point are introduced in each cell at the beginning, and all particle-points are tracked in the whole computation, and the information on the cell-point is determined as: if there are particle-points in current cell, the information is updated by averaging all particle-points' information; else if there are cell-points entered, the information is updated by averaging all entered cell-points' information; otherwise a new cell-point is set at the cell center and its transport value is obtained by interpolating those of contiguous cell-points. Different from the MAC method, the new method does not need cell classification and has only two times of the cell number's points to be stored. As it contains information on two kinds of Lagrangian points, we call it as dual information preserving (DIP) method. In addition, this paper developed a numerical perturbation method to solve the fractionated reaction step (ODE equation) to improve the stability and efficiency.

This paper is organized as follows. In section 2, we briefly introduce the decoupling method for solving the reactive Euler equations. In section 3, a dual information preserving method is proposed to solve the convection step of species mass fraction equations. In section 4, a numerical perturbation method is developed to solve the fractionated reaction step, analysis of stability and numerical examples are also presented. A series of examples, including one- and two- dimensional problems, simplified reaction model and multi-species reaction models, are given to validate the accuracy and robustness of the new method in section 5. Conclusions are shown in section 6.

2. Framework of the decoupling method for reactive Euler equations

The one-dimensional governing equations of reacting flows without considering of heat conduction and viscosity is given as

$$\frac{\partial U}{\partial t}+\frac{\partial F}{\partial x}=S, \tag{2.1}$$

where

$$U=\begin{pmatrix}\rho\\ \rho u\\ E\\ z_1\\ z_2\\ \vdots\\ z_{ns-1}\end{pmatrix}, F=\begin{pmatrix}\rho u\\ \rho u^2+p\\ u(E+p)\\ \rho z_1\\ \rho z_2\\ \vdots\\ \rho z_{ns-1}\end{pmatrix}, S=\begin{pmatrix}0\\ 0\\ 0\\ \omega_1\\ \omega_2\\ \vdots\\ \omega_{ns-1}\end{pmatrix},$$

ns is the number of reaction species, z_i and ω_i are the mass fraction and the production rate of ith species. The mass fraction of the nsth species is given by

$$z_{ns} = 1 - \sum_{i=1}^{ns-1} z_i.$$

And the pressure is

$$p = (\gamma - 1)(E - \frac{1}{2}\rho u^2 - \rho \sum_{i=1}^{ns} q_i z_i),$$

where q_i is the molar formation enthalpy of i species.

Eq.(**??**) is decoupled into two parts, the Euler equations

$$\frac{\partial U_1}{\partial t} + \frac{\partial F_1}{\partial x} = 0, \tag{2.2}$$

and the species equations in non-conservation form

$$\frac{\partial Z}{\partial t} + u\frac{\partial Z}{\partial x} = S_e, \tag{2.3}$$

where

$$U_1 = \begin{pmatrix} \rho \\ \rho u \\ E \end{pmatrix}, F_1 = \begin{pmatrix} \rho u \\ \rho u^2 + p \\ u(E+p) \end{pmatrix},$$

$$Z = \begin{pmatrix} z_1 \\ z_2 \\ \vdots \\ z_{ns-1} \end{pmatrix}, S_e = \begin{pmatrix} \omega_1/\rho \\ \omega_2/\rho \\ \vdots \\ \omega_{ns-1}/\rho \end{pmatrix}.$$

The Euler equations (**??**) can be solved by using conventional numerical method. In this paper, the Lax-Friedrichs flux splitting, the fifth-order weighted essentially non-oscillatory(WENO) scheme[**?**] and the fourth-order Runge-Kutta scheme[**?**] are used for the spatial discretization and temporal discretization, respectively.

Eq.(**??**) can be called the species equations, and it is further split into convection step

$$\frac{\partial Z}{\partial t} + u\frac{\partial Z}{\partial x} = 0, t_n \leqslant t \leqslant t_{n+1}, \tag{2.4}$$

and reaction step

$$\frac{dZ}{dt} = S_e, t_n \leqslant t \leqslant t_{n+1}. \tag{2.5}$$

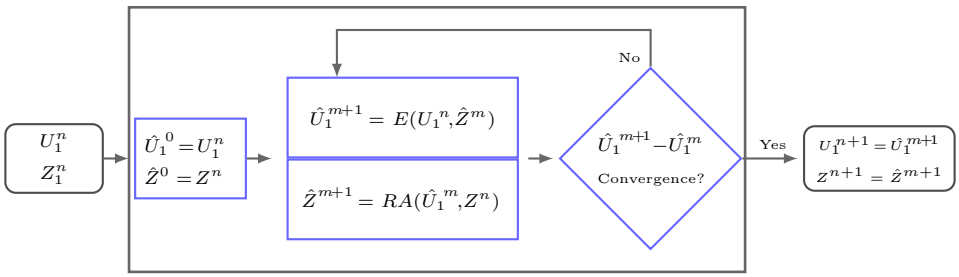

Figure 1: The framework of the solving process for the decoupling method.

The numerical solution at $n+1$ time step is obtained by

$$Z^{n+1} = RA(\hat{U}_1{}^m, Z^n). \tag{2.6}$$

The framework for solving the whole governing equations are shown in Fig.**??**. The variable $\hat{U}_1{}^m$ in Eq.(**??**) is the intermediate value calculated by Eq.(**??**). E, A and R denote the operators for solving the Euler equations (**??**), the convection equation (**??**) and the reaction equation (**??**) on the time interval $[t_n, t_{n+1}]$, respectively.

In the next two sections, we will introduce the new methods, i.e., the dual information preserving (DIP) method and the numerical perturbation (NP) method, for solving the convection equations (**??**) and reaction equations (**??**), respectively.

3. Dual Information Preserving method

The numerical stiff problems may be generated in simulating the chemical reacting flows due to the difference between the timescales in convection and chemical reaction, if there exist shock waves, the application of shock capturing schemes makes the problem more complex. In this section, a new method is proposed to cure the stiff problem, especially for that caused by the numerical dissipation generated by the strong shock capturing in chemical flows.

The two dimensional convection equation

$$\frac{\partial z}{\partial t} + u\frac{\partial z}{\partial x} + v\frac{\partial z}{\partial y} = 0. \tag{3.1}$$

is taken as an example to describe the numerical method.

There are two comments for this method:

Dual information: means the information on two different kinds of Lagrangian points (cell-points and particle-points).

Information: includes the transport value and the relative coordinates to the center of the Eulerian cell containing the virtual point.

The main idea of DIP is described as below:

(1) One Lagrangian particle-point and one Lagrangian cell-point are introduced in each Eulerian cell

at the beginning. The locations of all points are updated by using the velocity field (obtained from the computation of the Euler equation).

(2) For cell-point: if there are particle-points in the current cell, the information is updated by averaging all particle-points' information; else if there are cell-points entered, the information is updated by averaging all entered cell-points' information; otherwise a new cell-point is set at the cell center and its transport value is obtained by interpolating those of two nearest cell-points along the velocity direction.

(3) Transport values of two kinds of points are updated by solving the reaction equation.

(4) The transport value of the cell-point is used as the current cell's value for solving the equation of state.

Clearly, there is only one cell-point in each cell after a time step, and the particle-points are tracked and preserved all the time except those moved out of the computation domain.

The detailed algorithm is given in Appendix I.

3.1. Numerical test for the DIP method

In this subsection, we test the capability of the DIP method in discontinuities/interface cases.

Example 3.1.

The linear equation

$$\frac{\partial u}{\partial t}+\frac{\partial u}{\partial x}=0,$$

with following initial condition is solved as the first example to test the DIP algorithm.

$$u_0(x)=\begin{cases}\frac{1}{6}\left(G(x,\beta,z-\delta)+G(x,\beta,z+\delta)+4G(x,\beta,z)\right), & -0.8\leqslant x\leqslant -0.6,\\ 1, & -0.4\leqslant x\leqslant -0.2,\\ 1-|10(x-0.1)|, & 0\leqslant x\leqslant 0.2,\\ \frac{1}{6}\left(F(x,\alpha,a-\delta)+F(x,\alpha,a+\delta)+4F(x,\alpha,a)\right), & 0.4\leqslant x\leqslant 0.6,\\ 0, & otherwise,\end{cases} \tag{3.2}$$

and

$$G(x,\beta,z)=exp(-\beta(x-z)^2),$$

$$F(x,\gamma,a)=\sqrt{max(1-\alpha^2(x-a^2),0)}.$$

Where $a=0.5$, $z=-0.7$, $\delta=0.05$ and $\beta=log2/3\delta^2$. The grid number is $N=200$. Fig.**??** gives the comparison of the results of the fifth-order WENO scheme and the DIP method. For the linear equation, as the velocity is constant, the DIP method is a Lagrangian point tracking method, and hence there is no numerical dissipation introduced in the propagation process. The solution obtained by the DIP method is the exact solution.

Figure 2: Numerical solution of Example **??**, T=6, CFL=0.6.

Example 3.2.

The inviscid Burgers equation is calculated as the second example.

$$\frac{\partial u}{\partial t} + u\frac{\partial u}{\partial x} = 0, u_0(x) = sin(\pi x), 0 \leq x \leq 2. \tag{3.3}$$

Fig.**??** shows the results at $T = 0.4$ with $N = 200$. It can be seen that, for nonlinear convection equation, even if the initial condition is a smooth solution, the discontinuity is generated with time advancing. The numerical results show that the DIP method can capture this kind of discontinuity well.

Example 3.3.

Zalesak's disk [**?**] is a classical example to exam the capability of interface-tracking of a method[**?**]. The governing equation is a 2D scalar equation

$$\frac{\partial u}{\partial t} + v_x\frac{\partial u}{\partial x} + v_y\frac{\partial u}{\partial y} = 0. \tag{3.4}$$

The velocity field is taken as

$$\begin{cases} v_x(x,y) &= 2\pi y, \\ v_y(x,y) &= -2\pi x, \end{cases}$$

Figure 3: Numerical solution of Example **??**, T=0.4, CFL=0.6.

and the initial conditions are

$$u(x,y) = \begin{cases} 0, & \sqrt{x^2+y^2} > 0.4, \\ 0, & 0.4 < y < 0.6 and x > 0.5, \\ 1, & else. \end{cases}$$

The computation domain is $[0,1] \times [0,1]$. Fig.**??** shows the results at the time ($T_1 = 0$, $T_2 = 0.25$, $T_3 = 0.5$, $T_4 = 0.75$, $T_5 = 1$ and $T_6 = 20$) with $N = 200 \times 200$. The DIP method can keep the shape of the disk well.

Example 3.4.

Using the same equation (**??**), another 2D interfacial problem is calculated[**? ?**]. At the initial time, a circle with the radius of 0.2 is located at

$$u(x,y) = \begin{cases} 1, & \sqrt{(x-0.5\pi)^2 + (y-0.7)^2} \leqslant 0.2, \\ 0, & else. \end{cases}$$

The velocity field is taken as

$$\begin{cases} v_x(x,y) &= cos(x-0.5\pi)sin(y-0.5\pi), \\ v_y(x,y) &= -sin(x-0.5\pi)cos(y-0.5\pi). \end{cases}$$

The computation domain is $[0,\pi] \times [0,\pi]$. The interface is stretched up to time $T = t/2$, and then is brought back to its initial configuration at time $T = t$. Fig.**??** shows the results at the time $t = 2\pi$ and

Figure 4: Numerical results of Example **??** with $N = 200 \times 200$ at different time ($T_1 = 0$, $T_2 = 0.25$, $T_3 = 0.5$, $T_4 = 0.75$, $T_5 = 1$ and $T_6 = 20$). The exact initial value is given by the black line.

$t = 8\pi$ with $N = 200 \times 200$. The shape of the circle at the time $T = t$ is in agreement well with the initial shape even after a long time.

4. Numerical perturbation method for reactive ordinary differential equations

The NP method is first proposed by Gao[**?** **?**] to solve the convective-diffusion equations. The main idea of constructing the algorithm is as follows: the coefficient of the convective derivative in the basic discretization schemes (the first-order upwind scheme, the second-order central scheme) are reconstructed as a power-series of grid intervals; using the convective-diffusion equation itself, the high order mathematical relation is obtained; by eliminating truncated error terms in the modified differential equation of the reconstructed scheme, the coefficients in the power-series are determined and finally the numerical perturbation algorithms are obtained. In the fractional method, the reaction step forms a set of ordinary differential equations (ODE). In this section, we construct several efficient schemes for solving the reaction ODE based on the idea of numerical perturbation (NP).

4.1. The numerical perturbation schemes

Usually, the ODE equation is given as

$$\frac{dx}{dt} = f(t, x), x(0) = x_0, (x \in \mathbb{R}^s, t \leqslant 0). \tag{4.1}$$

$T = t/2 = \pi.$

$T = t = 2\pi.$

$T = t = 8\pi.$

$T = t/2 = 4\pi.$

Figure 5: Numerical results of Example **??**, $N = 200 \times 200$. The exact value is given by the black line.

The first-order explicit Euler scheme

$$x_{n+1} - x_n = \Delta t f(t, x_n), \tag{4.2}$$

is taken as the basic discretization scheme for the numerical perturbation. Applying Tayler expansion, we get the modified differential equation of Eq.(**??**) as

$$\frac{dx}{dt} = f(t,x) - \frac{1}{2}\Delta t \frac{d^2x}{dt^2} - O(\Delta t^2). \tag{4.3}$$

Similar as the construction of the numerical perturbation method for convective diffusion equation[**? ?**], a perturbation polynomial p is used to multiply the left of Eq.(**??**), i.e.,

$$p(x_{n+1} - x_n) = \Delta t f(t, x_n), \tag{4.4}$$

where the polynomial p is defined as

$$p = 1 + \sum_{i=1}^{\infty} a_i \Delta t^i. \tag{4.5}$$

Substituting Eq.(**??**) into Eq.(**??**) and using Taylor expansion, we get

$$\frac{dx}{dt} = f(t,x) - \left(\frac{1}{2}\frac{d^2x}{dt^2} + a_1\frac{dx}{dt}\right)\Delta t - \left(\frac{1}{6}\frac{d^3x}{dt^3} + \frac{a_1}{2}\frac{d^2x}{dt^2} + a_2\frac{dx}{dt}\right)\Delta t^2 + O\left(\Delta t^4\right). \tag{4.6}$$

Clearly, if the second term in the right hand side of Eq.(**??**) becomes zero,

$$\frac{1}{2}\frac{d^2x}{dt^2} + a_1\frac{dx}{dt} = 0, \tag{4.7}$$

then the scheme (**??**) has second-order accuracy. Similarly, we can get higher order schemes by eliminating more terms of Eq.(**??**). Since all derivatives can be calculated by using Eq.(**??**)

$$\frac{dx}{dt} = f, \frac{d^2x}{dt^2} = f'_t + f'_x f, \cdots .$$

We can find the perturbation coefficients as follows,

$$a_1 = -\frac{f'_t + f'_x f}{2f},$$

$$a_2 = \frac{-2f(f''_{tt} + 2f''_{tx}f + f'_x f'_t + f'_x f'_x f + f''_{xx}f^2) + 3(f'_t + f'_x f)^2}{12f^2},$$

$$\cdots$$

Specially, if f is the function only respecting to x, these coefficients a_i have simple formulas as follows,

$$a_1 = -\frac{f'}{2}, \quad a_2 = \frac{1}{12}f'^2 - \frac{1}{6}f''f, \quad \cdots . \tag{4.8}$$

For expressing conveniently, the perturbation polynomial for a Nth-order NP scheme is denoted as

$$p_N = 1 + \sum_{i=1}^{N-1} a_i \Delta t^i,$$

and the Nth-order NP scheme for the equation (**??**) can be written as

$$x_{n+1} = x_n + \Delta x f(t, x_n)/p_N. \tag{4.9}$$

In addition, we construct a transformed function to replace the original perturbation polynomial to improve the stability of the third-order NP(3NP) scheme. The function can be expressed as

$$\overline{p}_3 = \frac{1 + b_1\Delta t + b_2\Delta t^2}{1 - b_2\Delta t}, \tag{4.10}$$

Requiring $\overline{p}_3$ to be a second-order approximation of p_3 we get

$$b_1 = a_1 - \frac{a_2}{a_1 + 1}, \;\; b_2 = \frac{a_2}{a_1 + 1}. \tag{4.11}$$

The new third-order transformed NP (3TNP) scheme with the transformed function p_3 has third-order accuracy, but its stability region is larger than the 3NP scheme. The analysis and comparison will be given in the next subsection.

4.2. The stability analysis of the NP schemes

Stability is necessary and important for a scheme to solve the ODE equations system with stiffness[**?**]. Generally, the scalar equation

$$x' = qx, Re(q) < 0, \tag{4.12}$$

is used to study the stability. For a scheme, the solution of Eq.(**??**) can be expressed as

$$x_{n+1} = E(h)x_n, \tag{4.13}$$

where $h = q\Delta t$. The A-stability was proposed and used to analyze a numerical scheme in Refs.[**?** **?** **?**].

Two definitions for A-stability are given in Ref.[**?**]:

DEFINITION 1 (A-stable). *A scheme is A-stable, in the sense of Dahlquist[**?**], if $E(h) < 1$ for all complex h with negative real part.*

DEFINITION 2 (Strong A-stable). *A scheme is strongly A-stable, if it is A-stable and* $\lim_{Re(h)\to-\infty} E(h) = 0$.

In order to show the performance of the stability of NP schemes, several conventional schemes, include the first-order explicit Euler scheme (1EE), the first-order implicit Euler scheme (1IE), the second-order linearized implicit Euler scheme (2LIE) and the third-order explicit Runge-Kutta scheme (3RK), are analyzed and compared.

(1) The first-order explicit Euler scheme

$$x_{n+1} - x_n = \Delta t f(t, x_n), \tag{4.14}$$

and

$$E^{1EE}(h) = 1 + h. \tag{4.15}$$

(2) The first-order implicit Euler scheme

$$x_{n+1} - x_n = \Delta t f(t, x_{n+1}), \tag{4.16}$$

and

$$E^{1IE}(h) = \frac{1}{1-h}. \tag{4.17}$$

(3) The second-order linearized trapezoidal method [**? ?**]

$$x_{n+1} - x_n = \frac{\Delta t f(t, x_n)}{1 - 1/2\Delta t f'_x(t, x_n)}, \tag{4.18}$$

and

$$E^{2LIE}(h) = \frac{1 + \frac{1}{2}h}{1 - \frac{1}{2}h}. \tag{4.19}$$

Notice that, it has the same form as the 2NP scheme.

(4) The third-order explicit Runge-Kutta scheme

$$\begin{aligned} x_{n+1} &= x_n + \tfrac{1}{4}k_1 + \tfrac{3}{4}k_3, \\ k_1 &= \Delta t f(t_n, x_n), \\ k_2 &= \Delta t f(t_n + \tfrac{1}{3}\Delta t, x_n + \tfrac{1}{3}k_1), \\ k_3 &= \Delta t f(t_n + \tfrac{2}{3}\Delta t, x_n + \tfrac{2}{3}k_2), \end{aligned} \tag{4.20}$$

and

$$E^{3RK}(h) = 1 + h + \frac{1}{2}h^2 + \frac{1}{6}h^3. \tag{4.21}$$

For Eq.(**??**), it's easy to find the perturbation coefficients as $a_1 = -\frac{1}{2}q$, $a_2 = \frac{1}{12}q^2, \cdots$. Hence, the functions $E(h)$ for the NP schemes are

$$\begin{aligned} E^{2NP}(h) &= \frac{1 + \frac{1}{2}h}{1 - \frac{1}{2}h}, \\ E^{3NP}(h) &= \frac{1 + \frac{1}{2}h + \frac{1}{12}h^2}{1 - \frac{1}{2}h + \frac{1}{12}h^2}, \\ E^{3TNP}(h) &= \frac{1 + \frac{1}{3}h}{1 - \frac{2}{3}h + \frac{1}{6}h^2}. \end{aligned}$$

Fig.**??** gives the stable region for different schemes in the complex h plane. It shows that the first-order implicit, the second-order perturbation, the third-order NP and the transformed third-order NP schemes are A-stable. The transformed third-order NP scheme has a larger stable region than its counterpart, moreover, only this scheme and the first-order implicit Euler scheme are strongly A-stable schemes.

It is worthy to point out, different from the implicit schemes, the NP schemes do not need iterations and

Figure 6: Region of the stability in complex h plane for different schemes.

hence are more efficient.

4.3. Numerical comparison of different schemes

Before used to solve chemical equations, the stability and accuracy of perturbation schemes are tested and compared with other schemes used in ODEs.

Example 4.1.

$$\frac{dx}{dt} = f(t,x) = -50(x - \cos t). \tag{4.22}$$

This equation is calculated by Hairer[**?**] and used as the first case in this section. The perturbation coefficients in Eq.(**??**) are

$$a_1 = 25 - \frac{\sin t_n}{2(x_n - \cos t_n)}, \quad a_2 = \frac{1}{4}\left(\frac{\sin t_n}{x - \cos t_n} - 50\right)^2 - \frac{\cos t_n - 50\sin t_n}{6(x - \cos t_n)}.$$

Fig.**??** shows the results of different schemes. We can see the 1EE scheme and the 3RK schemes are not stable to solve Eq.(**??**). While the 2NP scheme has one point overshot. The 3NP, the 3TNP and the 1IE schemes are stable. It also can be seen that the 3NP and the 3TNP are more accuracy than the 1IE scheme.

Figure 7: Numerical results of Example **??**. Exact solution with $N = 3000$.

It should be noted that, although the implicit scheme can get a stable solution, they need iteration in every time step.

Example 4.2.

The equation

$$\frac{dx}{dt} = f(t, x) = -x^3, x_0 = 1, t = [0, 1], \tag{4.23}$$

is calculated as the second case. In this case, the analytic solution is

$$x = \frac{1}{\sqrt{2t+1}}.$$

The perturbation coefficients of the second-order and the third-order schemes are

$$a_1 = \frac{3x_n^2}{2}, a_2 = -\frac{x_n^4}{4}.$$

Table.**??** gives the errors and accuracy orders of different schemes. It shows that the second-order, the third-order and the transformed NP schemes can get their theoretical accuracy orders. The errors of the third-order NP and transformed NP schemes are lower than the third-order Runge-Kutta schemes, though all of them are third-order accuracy.

5. Applications in the reactive Euler equations

In this section we apply the methods proposed in Section 2-4 to solve various reactive problems.

Table 4.1: The accuracy of different schemes used in Example **??**.

Scheme	N	L_1 error	L_1 order	L_∞ error	L_∞ order
1IE	20	7.7149d-3	—	8.7737d-3	—
	40	3.9062d-3	0.98	4.4879d-3	0.97
	80	1.9656d-3	0.99	2.2712d-3	0.98
	160	9.8594d-4	1.00	1.1426d-3	0.99
	320	4.9377d-4	1.00	5.7304d-4	1.00
3RK	20	1.3696d-5	—	1.7438d-5	—
	40	1.6161d-6	3.08	2.0646d-6	3.08
	80	1.9601d-7	3.04	2.5119d-7	3.04
	160	2.4128d-8	3.02	3.0964d-8	3.02
	320	2.9924d-9	3.01	3.8433d-9	3.01
2NP	20	5.0683d-5	—	6.0346d-5	—
	40	1.2338d-5	2.04	1.4812d-5	2.03
	80	3.0414d-6	2.02	3.6679d-6	2.01
	160	7.5487d-7	2.01	9.1226d-7	2.01
	320	1.8803d-7	2.01	2.2750d-7	2.00
3NP	20	1.9980d-6	—	2.5388d-6	—
	40	2.3999d-7	3.06	3.0629d-7	3.05
	80	2.9376d-8	3.03	3.7628d-8	3.03
	160	3.6325d-9	3.03	4.6607d-9	3.01
	320	4.5143d-10	3.01	5.7972d-10	3.01
3TNP	20	1.8060d-6	—	2.2866d-6	—
	40	2.1766d-7	3.06	2.7702d-7	3.05
	80	2.6685d-8	3.03	3.4085d-8	3.02
	160	3.3025d-9	3.01	4.2255d-9	3.01
	320	4.1057d-10	3.01	5.2582d-10	3.01

5.1. Numerical examples for scalar problems

Example 5.1.

Consider a scalar model problem[**?**]

$$\frac{\partial u}{\partial t}+\frac{\partial u}{\partial x}=-\mu u(u-0.5)(u-1). \tag{5.1}$$

It's initial condition is given as

$$u_0(x)=\begin{cases}1, & x\leqslant 0.3,\\ 0, & x>0.3.\end{cases}$$

The exact solution is

$$u_0(x)=\begin{cases}1, & x\leqslant t+0.3,\\ 0, & x>t+0.3.\end{cases}$$

The source term should always be zero theoretically. However, if μ in Eq.(**??**) is very large, the wrong numerical result may appear in the transition region without a suitable method. Using the fractional method, the convection step

$$A:\frac{\partial u}{\partial t}+\frac{\partial u}{\partial x}=0, \qquad t_n\leqslant t\leqslant t_{n+1},$$

is solved by the DIP method and the reaction step

$$R:\frac{du}{dt}=f(u)=-\mu u(u-0.5)(u-1), \qquad t_n\leqslant t\leqslant t_{n+1},$$

is solved by the 3TNP scheme. For this case, it is easy to find the first-order and the second-order derivatives of f for calculating the perturbation coefficients.

Notice that, the scheme for ODE equations mainly influences the stability of computation and the time step (the CFL number). Due to its high order and stability, only the third-order transformed NP scheme is used in this paper.

Fig.**??** gives the numerical results calculated by the present method (DIP) and the WENO method for the non-stiff case $\mu=10$ and stiff case $\mu=10,000$. We can see the present method can resolve Eq.(**??**) with both cases, while the result calculated by the WENO method for the stiff case has a spurious propagation phenomenon.

5.2. Simplified reactive Euler system

In this system, the reaction has only two states, burnt and un-burnt. Un-burnt gas convert to burnt gas via a single irreversible reaction. The governing equation is Eq.(**??**), its mass fraction is controlled by a scalar equation

$$\frac{\partial z}{\partial t}+u\frac{\partial z}{\partial x}=s_1, \tag{5.2}$$

Figure 8: The numerical results of Example **??**, $t = 0.3$. Left:the non-stiff case; Right: the stiff case.

and the source term expresses as

$$s_1 = -K(T)z.$$

The reaction rate K determines the stiffness and can be modeled by the Arrhenius law

$$K(T) = K_0 exp(\frac{-T_{ign}}{T}),$$

or by the Heaviside law

$$K(T) = \begin{cases} 1/\epsilon, & T \geqslant T_{ign}, \\ 0, & T < T_{ign}, \end{cases}$$

where K_0 is the reaction rate constant, T_{ign} is the ignition temperature and ϵ is the reaction time.

Example 5.2.

The first example is an ozone decomposition Chapman-Jouguet (C-J) detonation, which has been computed and discussed in[**? ? ? ?**]. The Arrhenius source term is used with the following parameter values

$$(\gamma, q_0, K_0, T_{ign}) = (1.4, 0.5196 \times 10^{10}, 0.5825 \times 10^{10}, 0.1155 \times 10^{10}).$$

The initial values are piecewise constants with burnt gas on the left-hand side and un-burnt gas on the right-hand side, given as

$$(\rho, u, p, z) = \begin{cases} (\rho_b, u_b, p_b, 0), & x \leqslant 0.005, \\ (\rho_0, u_0, p_0, 1), & x > 0.005, \end{cases}$$

where $\rho_0 = 1.201 \times 10^{-3}$, $p_0 = 8.321 \times 10^5$ and $u_0 = 0$. The states of the C-J initial burnt gas are obtained

by[**?** **?** **?** **?**]

$$\begin{aligned} p_b &= -b + (b^2 - c)^{1/2}, \\ \rho_b &= \rho_u[p_b(\gamma+1) - p_u]/(\gamma p_b), \\ S_{cj} &= [\rho_0 u_0 + (\gamma p_b \rho_b)^{1/2}]/\rho_0, \\ u_b &= S_{cj} - (\gamma p_b/\rho_b)^{1/2}, \\ b &= -p_u - \rho_u q_0(\gamma - 1), \\ c &= p_u^2 + 2(\gamma-1)p_u\rho_u q_0/(\gamma+1), \end{aligned} \tag{5.3}$$

where S_{cj} is the speed of the detonation front.

This problem is solved on the interval $[0, 0.05]$. The "exact" solutions are obtained by using the direct WENO method in a refined mesh with the size $\Delta x = 5 \times 10^{-6}$ (i.e., $N = 10,000$), which is suggested to resolve the reaction scale[**?** **?** **?**]. In this paper, as those methods are called as "the standard method" in Refs. [**?** **?** **?**], "the direct WENO method" means using the fifth-order WENO scheme [**?**] and the fourth-order Runge-Kutta method[**?**] to discretize the spatial derivatives and temporal derivatives in the homogeneous Euler equations (Eq.(**??**) without source term) in the conventional fractional-step method, and the same 3TNP method is used to solve the reaction equation. The results obtained by the direct WENO method is symboled as "WENO" in all figures.

The solutions at the time $t = 3 \times 10^{-7}$ with two meshes of $N = 50$ and $N = 300$ are displayed in Fig.**??** and Fig.**??**, respectively. They show that, the present method can capture the correct profile of detonation wave even the coarse mesh $N = 50$ is used, while applying the direct WENO method, a spurious weak detonation appears ahead of the detonation wave.

Kotov et al. [**?**] shown that the spurious behavior is influenced significantly by the CFL number, and increasing the stiffness coefficient may generate large derivation for predicting the shock location. To test the influence of the CFL on the new method , we change K_0 to $100K_0$. Three different meshes of $N = 50, N = 100$ and $N = 300$ are used. Numerical results show that the influence of the CFL number on the new method can be neglected. Fig.**??** gives the pressure and the mass fraction distribution of $N = 300$ obtained by the new method.

In this example, we also test the convergence of the iteration in the decoupling process, which is given in the framework of the solving process in Fig.**??**. The error is measured by

$$error = \frac{|u^{m+1} - u^m|}{dt}, \tag{5.4}$$

and used to estimate the convergence rate. The convergence history is plotted in Fig.**??**. It can be seen that, the iteration is converged only a few steps. Our numerical tests also show that the difference between the results by using different iteration steps can be neglected, hence, in this paper, only one step is adopt.

Example 5.3.

This is another C-J detonation, in which the Heaviside source term[**?** **?** **?**] with the following parameters

Figure 9: Numerical results of Example **??**, $T = 3 \times 10^{-7}$, $N = 50$.

Figure 10: Numerical results of Example **??**, $T = 3 \times 10^{-7}$, $N = 300$.

Figure 11: Numerical results of Example **??** with $100/\epsilon$, $T = 3 \times 10^{-7}$, $N = 300$.

Figure 12: Convergence history of Example **??**.

is used,

$$(\gamma, q_0, K_0, T_{ign}) = (1.4, 25, 16418, 25).$$

The initial conditions are

$$(\rho, u, p, z) = \begin{cases} (\rho_b, u_b, p_b, 0), & x \leqslant 10, \\ (1, 0, 1, 1), & x > 10. \end{cases}$$

The burnt states are calculated by using the same formula Eq.(**??**).

The results with $N = 50$ and $N = 300$ are shown in Fig.**??** and Fig.**??**, respectively. The "exact" solution is solved by the direct WENO method with $N = 10,000$. The new method can capture the correct speed of the strong detonation wave even with the coarse mesh.

Example 5.4.

In this example, we considered a detonation case with more complex waves[**? ? ? ?**]. And the Heaviside model with following parameters are used,

$$(\gamma, q_0, 1/\epsilon, T_{ign}) = (1.2, 50, 230.75, 3).$$

The initial conditions of this example are

$$(\rho, u, p, z) = \begin{cases} (2, 4, 40, 0), & x \leqslant 10, \\ (3.64282, 6.2489.54.8244, 0), & 10 < x \leqslant 20, \\ (1, 0, 1, 1), & x > 20. \end{cases}$$

The solution contains a right moving strong detonation, a right moving rarefaction wave, a right moving contact discontinuity and a left moving rarefaction wave. The "exact" solution is obtained with $N = 10,000$. The results at the final time $T = 8$ with $N = 50$ and $N = 300$ (with $100/\epsilon$) are plotted in Fig.**??** and Fig.**??**. It can be seen that the DIP method can capture different structures well, even in the case with more complex waves and more serious stiffness, while the direct WENO method still cannot obtain the correct location of detonation front.

Example 5.5.

The last one-dimensional problem in this subsection involves a collision with an oscillatory profile[**? ?**]. The parameters for the Heaviside model are

$$(\gamma, q_0, 1/\epsilon, T_{ign}) = (1.2, 50, 1000, 3).$$

And the initial conditions are given as

$$(\rho, u, p, z) = \begin{cases} (1.79463, 3.0151, 21.53134, 0), & x \leqslant \frac{\pi}{2}, \\ (3.64282, 6.2489.54.8244, 0), & x > \frac{\pi}{2}. \end{cases}$$

Figure 13: Numerical results of Example **??**, $T = 1.8$, $N = 50$.

Figure 14: Numerical results of Example **??**, $T = 1.8$, $N = 300$.

Figure 15: Numerical results of Example **??** with $100K_0$, $T = 1.8$, $N = 300$.

Similarly, the results of the direct WENO method with $N = 10,000$ are taken as the "exact" solution. Fig.**??** gives the comparison at $t = \pi/2$ with the mesh $N = 300$. It shows that the present method can not only capture the shocks well, but also obtains good resolution in smooth regions.

Example 5.6.

This is a two-dimensional detonation problem containing a moving detonation wave travels from left to right in a rectangular channel[**?** **?** **?**]. In this example, the Arrhenius source model is used and the parameters $\gamma, q_0, K_0, T_{ign}$ are the same as those in Example **??**. The initial conditions are given as

$$(\rho, u, v, p, z) = \begin{cases} (\rho_b, u_b, 0, p_b, 0), & x \leqslant \xi(y), \\ (1.201 \times 10^{-3}, 0, 0, 8.321 \times 10^5, 1), & x > \xi(y), \end{cases}$$

$$\xi(y) = \begin{cases} 0.004, & |y - 0.0025| \geqslant 0.001, \\ 0.005 - |y - 0.0025|, & |y - 0.0025| < 0.001. \end{cases}$$

Where ρ_b, u_b and p_b are also calculated by Eq.(**??**).

The "exact" solution is computed by the direct WENO method with $N = 2000 \times 400$. Fig.**??** gives the density contours at the beginning and the final time ($t = 1.4 \times 10^{-7}$) with the refined mesh. Fig.**??** displays the density contours at time ($T = 0$, $T_1 = 0.28 \times 10^{-7}$, $T_2 = 0.7 \times 10^{-7}$, $T_3 = 1.12 \times 10^{-7}$ and $T_4 = 1.4 \times 10^{-7}$) with two meshes of $N = 150 \times 50$ and $N = 600 \times 200$. It can be seen that, the shock locations captured with different meshes agree well, and the flow structures are also resolved well even with coarse mesh. The distributions of $N = 600 \times 200$ on the line of $y = 0.0025$ are also given in Fig.**??**, which shows that, the

Figure 16: Numerical results of Example **??**, $T = 8$, $N = 50$.

Figure 17: Numerical results of Example **??** with $100/\epsilon$, $T = 8$, $N = 300$.

Figure 18: Numerical results of Example **??**, $T = \pi/2$, $N = 300$.

detonation wave computed by the present method has a good agreement with the reference solution, while the direct WENO method generates unphysical results similar to that in one-dimensional examples.

Example 5.7.

This is another two-dimensional detonation wave problem taken from Ref.[**? ?**]. The following parameters are used for modeling the Heaviside source term,

$$(\gamma, q_0, K_0, T_{ign}) = (1.2, 50, 1000, 2).$$

The initial conditions are given as

$$(\rho, u, v, p, z) = \begin{cases} (1.79463, 10x/r, 10y/r, 21.53134, 0), & r \leqslant 10, \\ (1, 0, 0, 1, 1), & r > 10, \end{cases}$$

where

$$r = \sqrt{x^2 + y^2}.$$

This problem represents a radial symmetrical detonation wave moving in a rectangular region. The "exact" solution is computed by the direct WENO method with a refined mesh of $N = 1000 \times 500$. The detonation front with the mesh $N = 200 \times 100$ at time $T_1 = 0$, $T_2 = 1$, $T_3 = 3$ and $T_4 = 5$ are shown in Fig.**??**. We can see the present method can capture the location of the detonation front exactly. Fig.**??** compares the results at the time $T = 5$. The present method obtained the same discontinuity location for pressure, density, temperature and mass fraction, but using the direct WENO method, the mass fraction displays a different behavior due to the stiffness, in addition, the distributions of pressure, density and temperature are also distorted compared to the "exact" solution.

5.3. Multi-specise reactive Euler system

For multi-species reactive Euler equations without heat conduction and viscosity, the decoupled species equations are in the form of

$$\frac{\partial Z}{\partial t} + u\frac{\partial Z}{\partial x} = S_e,$$

where

$$Z = \begin{pmatrix} z_1 \\ z_2 \\ \vdots \\ z_{ns-1} \end{pmatrix}, S_e = \begin{pmatrix} s_1 \\ s_2 \\ \vdots \\ s_{ns-1} \end{pmatrix},$$

with the source terms given as

$$s_i = \frac{W_i}{\rho} \sum_{k=1}^{nr} (\mu''_{i,k} - \mu''_{i,k}) K_k \prod_{j}^{ns} \left(\frac{\rho z_j}{W_j}\right)^{\mu'_{j,k}},$$

Figure 21: The distributions on the line $y = 0.0025$ of Example **??**, $T = 1.4 \times 10^{-7}$

Figure 22: Mass fraction ($z = 0.5$) of Example **??**.

Figure 23: Comparison of the numerical results on the diagonal line, Example **??**, $T = 5$.

where nr is the number of reactions

$$z_{ns} = 1 - \sum_{i=1}^{ns-1} z_i.$$

And the pressure is given by

$$p = (\gamma - 1)\left(e - \frac{1}{2}\rho u^2 - q_1\rho z_1 - q_2\rho z_2 - \cdots - q_{ns}\rho z_{ns}\right).$$

The temperature is defined as $T = p/\rho$. The reaction rate of the irreversible chemical reaction K_i determines the stiffness of the problem and is expressed in the Heaviside form

$$K_i(T) = \begin{cases} 1/\epsilon_i, & T \geqslant T_{ign}, \\ 0, & T < T_{ign}. \end{cases} \qquad i = 1, 2, \cdots, nr$$

The transformed third-order perturbation scheme is

$$z_{i,j}^{n+1} = z_{i,j}^n + \frac{1}{\bar{p_i}}\Delta t s_i(z_{i,j}^n), \qquad i = 1, 2, \cdots, ns-1$$

and

$$\bar{p_i} = \frac{1 + b_{i,1}\Delta t + b_{i,2}\Delta t^2}{1 - b_{i,2}\Delta t},$$

where

$$b_{i,1} = a_{i,1} - \frac{a_{i,2}}{a_{i,1}+1}, \quad b_{i,2} = \frac{a_{i,2}}{a_{i,1}+1},$$

and

$$a_{i,1} = -\frac{1}{2}\sum_{j=1}^{ns}\frac{\partial s_i}{\partial z_j}s_j/s_i,$$

$$a_{i,2} = -\frac{1}{6}\sum_{j=1}^{ns}\sum_{k=1}^{ns}\left(\frac{\partial^2 s_i}{\partial z_j \partial z_k}s_j s_k + \frac{\partial s_i}{\partial z_j}\frac{\partial s_j}{\partial z_k}s_k\right)/s_i + a_{i,1}^2.$$

In this paper, a numerical approximation is used

$$\frac{\partial s_i}{\partial z_j} = \frac{s_i(z_j + \Delta z) - s_i(z_j)}{\Delta z},$$

where Δz is a small value compared to z_j, and taken as

$$\Delta z = \begin{cases} z_j/100, & z_j \neq 0, \\ 0.001, & z_j = 0. \end{cases}$$

Example 5.8.

The first multi-species example is taken from[**?** **?**], it uses a simple reaction model

$$2H_2 + O_2 \to 2H_2O.$$

The parameters for the Heaviside source term are

$$(\gamma, T_{ign}, 1/\epsilon, q_{H_2}, q_{O_2}, q_{H_2O}, W_{H_2}, W_{O_2}, W_{H_2O}) = (1.4, 2, 10^6, 100, 0, 0, 2, 32, 18).$$

And the initial values are given as following

$$(\rho, u, p, z_{H_2O}, z_{O_2}, z_{H_2O}) = \begin{cases} (2, 8, 20, 0, 0, 1), & 0 \leqslant x \leqslant 2.5, \\ (1, 0, 1, 1/9, 8/9, 0), & 2.5 < x \leqslant 50. \end{cases}$$

The "exact" solution is computed by the direct WENO method with a refined mesh of $N = 10,000$. The results of $N = 200$ at $T = 4$ are plotted in Fig.**??**. It shows that both the methods can capture the correct propagation wave. However, if the value of q_{H_2} changes from 100 to 300, as used in [**?**], the results plotted in Fig.**??** shows that the WENO method cannot maintain the correct propagation speed, while the present method still performs well.

Example 5.9.

This example has been studied in[**?**], its reaction model is

$$CH_4 + 2O_2 \to CO_2 + 2H_2O.$$

The following parameters are used for modeling the Heavisive source term,

$$(\gamma, T_{ign}, 1/\epsilon, q_{CH_4}, q_{O_2}, q_{CO_2}, q_{H_2O}) = (1.4, 2, 500, 100, 0, 0),$$

$$(W_{CH_4}, W_{O_2}, W_{CO_2}, W_{H_2O}) = (16, 32, 44, 18).$$

The initial conditions are

$$(\rho, u, p, z_{CH_4}, z_{O_2}, z_{CO_2}, z_{H_2O}) = \begin{cases} (2, 10, 40, 0.325, 0, 0, 0.675), & x \leqslant 2.5, \\ (1, 0, 1, 0.1, 0.4, 0.6, 0), & x > 2.5. \end{cases}$$

The solution of this problem consists of a detonation wave, followed by a contact discontinuity and a shock. The "exact" solution is computed with a refined mesh of $N = 10,000$. The results of $N = 200$ at $T = 3$ are displayed in Fig.**??**. It can be seen that, the solution obtained by the present method is in agreement well with the reference solution, while a deviated propagation speed is obtained by the direct WENO method.

Example 5.10.

The last one-dimensional multi-species example is taken from [**?** **?**]. The reaction model consists of five species and two reactions

$$H_2 + O_2 \to 2OH, \quad 2OH + H_2 \to 2H_2O.$$

Figure 24: Numerical results of Example **??**, $T = 4$ and $N = 200$. Top: the direct WENO method; Bottom: the present method.

Figure 25: Numerical results of Example **??** with $k_{H_2} = 300$, $T = 4$, $N = 200$.

Figure 26: Numerical results of Example **??**, $T = 3$, $N = 200$.

The species N_2 is used as a catalyst. All parameters given in [**?**] are

$$(\gamma, T_{ign}, 1/\epsilon_1, 1/\epsilon_2) = (1.4, 2, 10, 10^5, 2 \times 10^4),$$

$$(q_{H_2}, q_{O_2}, q_{OH}, q_{H_2O}, q_{N_2}) = (0, 0, -20, -100, 0),$$

$$(W_{H_2}, W_{O_2}, W_{OH}, W_{H_2O}, W_{N_2}) = (2, 32, 17, 18, 28).$$

And the initial conditions are

$$(\rho, u, p, z_{H_2}, z_{O_2}, z_{OH}, z_{H_2O}, z_{N_2}) = \begin{cases} (2, 10, 40, 0, 0, 0.17, 0.63, 0.2), & x \leqslant 0.5, \\ (1, 0, 1, 0.08, 0.72, 0, 0, 0.2), & x > 0.5. \end{cases}$$

The computation domain is $[0, 50]$. The "exact" solution is obtained with a refined mesh of $N = 10,000$. Fig.**??** gives the results of pressure, temperature, mass fractions of O_2 and OH. It shows that, with the parameters given by [**?**], both the two methods can get reasonable results, though the direct WENO method generates oscillation more clear than the present method.

The study shown that[**?**], with a smaller ignition temperature, the first reaction equation is easier to be activated, and hence the stiffness increased. Fig.**??** shows the results with $T_{ign} = 1.5$ and $q_{H_2} = -50$. For this case, the direct WENO method generates a bifurcating wave pattern and a faster propagation speed similar as the results in [**?**], while the present method can capture all waves with correct speeds.

Example 5.11.

The last case is a two-dimensional example, which has been studied in [**?**]. The source terms are calculated as those in Example **??**. The initial conditions are

$$(\rho, u, v, p, z_{H_2}, z_{O_2}, z_{OH}, z_{H_2O}, z_{N_2}) = \begin{cases} (2, 10, 0, 40, 0, 0, 0.17, 0.63, 0.2), & x \leqslant \xi(y), \\ (1, 0, 1, 0.08, 0.72, 0, 0, 0.2), & x > \xi(y), \end{cases}$$

where,

$$\xi(y) = \begin{cases} 12.5 - |y - 12.5|, & |y - 12.5| \geqslant 7.5, \\ 5, & |y - 0.0025| < 7.5. \end{cases}$$

The compute domain is $[0, 150] \times [0, 25]$. Fig.**??** shows the evolution of the detonation wave at time $T_1 = 0, T_2 = 2, T_3 = 4, T_4 = 6$ and $T_5 = 8$ with a mesh $N = 300 \times 50$. In order to compare, the results simulated by the direct WENO method with a refined mesh of $N = 1500 \times 250$ are also plotted. This figure shows the present method can resolve all the structures, even using a coarse mesh. Fig.**??** gaves the numerical comparison on the line of $y = 12.5$. The results obtained by the new method agree well with the "exact" solution.

Figure 27: Numerical results of Example **??**, $T = 3$, $N = 200$. Top: the direct WENO method; Bottom: the present method.

Figure 28: Numerical results of Example **??** with $T_{ign} = 1.5$ and $q_{H_2} = -50$. $T = 3$, $N = 200$.

Figure 30: Distribution on the line of $y = 12.5$ for Example **??** at $T = 8$, $N = 300 \times 50$.

6. Conclusions

The dual information preserving method is firstly proposed to cure the numerical stiff problem generated in simulating the reacting flows. First, the species mass fraction equations are decoupled from the reactive Euler equations, and then they are further fractionated into the convection step and reaction step. The DIP method is actually proposed to deal with the species convection step. Two kinds of virtual Lagrangian point are introduced, one is limited in each Eulerian cell, and another one is tracked in the whole computation domain. The number of each kind of virtual point is the same as the cell (grid) number.The DIP method can effectively eliminate the spurious propagation speed caused by the intermediate state generated by the numerical dissipation.

In this paper, the numerical perturbation (NP) methods are also developed to solve the fractionated reaction step (ODE equations). The NP schemes show several advantages, such as no iteration, high order accuracy and large stable region.

A series of numerical examples are used to demonstrate the reliability and robustness of the new methods.

Acknowledgement

This research work was supported by NSFC 11272324, 11272325, NSAF U1530145 and 2016YFA0401200.

References

Appendix A. The algorithm of the DIP method for solving the convection equations

(0) Initiation

$$\begin{cases} X(i,j)=0 \\ Y(i,j)=0 \end{cases},\begin{cases} X_p(i,j)=0 \\ Y_p(i,j)=0 \end{cases},\begin{cases} I(i,j)=i \\ J(i,j)=j \end{cases},\begin{cases} \hat{z}(i,j)=z(i,j) \\ z_p(i,j)=z(i,j) \end{cases}$$

DO $it=1,NT$! Time-Stepping

Solving the decoupled Euler equations (**??**) to get u, v, $\cdots$

Following is the DIP algorithm for the convection equations (**??**).

(1) Initial values

$Mrk(i,j)=0, S_1(i,j)=0, S_2(i,j)=0$

(2) Calculate the cell-point

DO $i=0,NX$

DO $j=0,NY$

$s_x=sign(X(i,j)), s_y=sign(Y(i,j))$

$$\begin{cases} u_c(i,j)= & (1-|X|)u(i,j) & +|X|u(i+s_x,j) \\ v_c(i,j)= & (1-|Y|)v(i,j) & +|Y|v(i,j+s_y) \end{cases}$$! Interpolating velocity according to its location

$$\begin{cases} L_x=X(i,j)+u_c(i,j)\Delta t/\Delta x \\ L_y=Y(i,j)+v_c(i,j)\Delta t/\Delta y \end{cases}$$

$$\begin{cases} M=i+floor(L_x+0.5) \\ N=j+floor(L_y+0.5) \end{cases}$$! (i,j) moves to cell (M,N)

$$\begin{cases} X(i,j)=L_x-floor(L_x+0.5) \\ Y(i,j)=L_y-floor(L_y+0.5) \end{cases}$$! The relative location in (M,N)

IF $(0\leqslant M\leqslant NX$ and $0\leqslant N\leqslant NY)$ Then

$Mrk(M,N)=1$

$S_1(M,N)=S_1(M,N)+1$

$$\begin{cases} \hat{X}(M,N)= & \{[S_1(M,N)-1]X(M,N) & +X(i,j)\}/S_1(M,N) \\ \hat{Y}(M,N)= & \{[S_1(M,N)-1]Y(M,N) & +Y(i,j)\}/S_1(M,N) \\ \hat{z}(M,N)= & \{[S_1(M,N)-1]z(M,N) & +\hat{z}(i,j)\}/S_1(M,N) \end{cases}$$! Averaging information

ENDIF

END DO

END DO

$$\begin{cases} X(:,:)=\hat{X}(:,:) \\ Y(:,:)=\hat{Y}(:,:) \end{cases}$$

(3) Calculate the particle-point and update the cell-point(I,J)

DO $i=0,NX$

DO $j=0,NY$

$s_x=sign(X_p(i,j)), s_y=sign(Y_p(i,j))$

$$\begin{cases} u_p(i,j)= & (1-|X_p|)u(I,J) & +|X|u(I+s_x,J) \\ v_p(i,j)= & (1-|Y_p|)v(I,J) & +|Y|v(I,J+s_y) \end{cases}$$! Interpolating velocity according to its position

$$\begin{cases} L_x=X_p(i,j)+u_p(i,j)\Delta t/\Delta x \\ L_y=Y_p(i,j)+v_p(i,j)\Delta t/\Delta y \end{cases}$$

$$\begin{cases} I(i,j)=I(i,j)+floor(L_x+0.5) \\ J(i,j)=J(i,j)+floor(L_y+0.5) \end{cases}$$! (i,j) moves to cell (I,J)

$$\begin{cases} X_p(i,j)=L_x-floor(L_x+0.5) \\ Y_p(i,j)=L_y-floor(L_y+0.5) \end{cases}$$! The relative location in (I,J)

IF $(0\leqslant I\leqslant NX$ and $0\leqslant J\leqslant NY)$ Then

$Mrk(I,J)=2$

$S_2(I,J)=S_2(I,J)+1$

$$\begin{cases} \hat{X}(I,J)= & \{[S_2(I,J)-1]X(I,J) & +X(i,j)\}/S_2(I,J) \\ \hat{Y}(I,J)= & \{[S_2(I,J)-1]Y(I,J) & +Y(i,j)\}/S_2(I,J) \\ \hat{z}(I,J)= & \{[S_2(I,J)-1]z(I,J) & +z_p(i,j)\}/S_2(I,J) \end{cases}$$! Updating cell-point (I,J)'s information by averaging all entered particle-points' information

END IF

END DO

END DO

$$\begin{cases} X(:,:)=\hat{X}(:,:) \\ Y(:,:)=\hat{Y}(:,:) \end{cases}$$

(4) If there is no cell-point in the cell (i,j), i.e, $Mrk(i,j)=0$

DO $i=0,NX$

DO $j=0,NY$

IF $Mrk(i,j)=0$ then

$$\begin{cases} X(i,j)=0 \\ Y(i,j)=0 \end{cases}$$

IF $|u(i,j)|\geqslant|v(i,j)|$ then ! Assigning new value by interpolating on x-direction

Finding the nearest two points $(i-il,j)$ and $(i+ir,j)$

$L=|X(i-il,j)-il)u(i,j)+Y(i-il,j)v(i,j)|$

$R = |X(i + ir, j) - ir)u(i, j) + Y(i + ir, j)v(i, j)|$
$\hat{z}(i, j) = [R\hat{z}(i - il, j)) + L\hat{z}(i + ir, j)]/(R + L)$

ELSE ! Assigning new value by interpolating on y-direction

Finding the nearest two points $(i, j - jl)$ and $(i, j + jr)$

$L = |X(i, j - jl)u(i, j) + (Y(i, j - jl) - jl)v(i, j)|$
$R = |X(i, j + jr))u(i, j) + (Y(i, j + jr) - jr)v(i, j)|$
$\hat{z}(i, j) = [R\hat{z}(i, j - jl)) + L\hat{z}(i, j + jr)]/(R + L)$

END IF
END IF
END DO
END DO

Solving the reaction equations (**??**) to get new z and z_p by using $\hat{z}$ and z_p to calculate the source terms, respectively.

END DO